BAYWOOD REPRINTS

JOURNAL OF
APPLIED FIRE SCIENCE

EXECUTIVE EDITOR: PAUL R. DECICCO

Volume 11, Number 4 – 2002-2003

Nonlinear Thin Shell Finite Element for Steel and Concrete Structures Subjected to Fire: Theoretical Development

Didier Talamona and Jean-Marc Franssen

BAYWOOD PUBLISHING COMPANY, INC.

J. APPLIED FIRE SCIENCE, Vol. 11(4) 291-310, 2002-2003

NONLINEAR THIN SHELL FINITE ELEMENT FOR STEEL AND CONCRETE STRUCTURES SUBJECTED TO FIRE: THEORETICAL DEVELOPMENT*

DIDIER TALAMONA
FireSERT, University of Ulster, United Kingdom

JEAN-MARC FRANSSEN
M&S, University of Liege, Belgium

ABSTRACT

This article describes the features of a quadrilateral thin shell element, based on Marguerre's theory that has been implemented in the finite element program SAFIR (from the University of Liege.) The element has four nodes (one at each corner) and each node has six degrees of freedom, i.e., three translations and three rotations (the sixth degree of freedom is a true one, which can be assimilated to the in-plane rotation.) This article presents some theoretical developments regarding the element formulation. The algorithm strategies for isotropic material (steel for example) and non-isotropic material (concrete) and their modifications for elevated temperatures are described. Two verifications examples are presented (the patch test and Lee's frame at elevated temperatures).

INTRODUCTION

Sophisticated and user-friendly programs have been developed over the last 20 to 30 years. The use of finite element programs has largely increased with the

*This workshop was supported by the European Commission through the *Marie Curie* fellowship granted to Dr. Talamona (contract number ERBFMBICT983336).

improvement of the capabilities of computers. The commercial programs are more and more user-friendly; nevertheless, they still require a high degree of expertise from the users. A large number of finite element types are usually available in these programs and the proper element has to be used depending on the structure to be meshed. This requires a good understanding of the physical problem (i.e., structural behavior) and a perfect knowledge of the capabilities and limitations of the finite elements used from the library of the software. On the one hand, commercial software is heavy to use when the problem of structures subjected to fire has to be tackled and, on the other hand, software dedicated to fire (developed by research labs or universities) is not so user friendly but is more flexible than commercial programs.

Franssen, from the University of Liege, developed SAFIR in the 90s. This finite element program is used for the thermal and mechanical analysis of structures submitted to fire. Thermal calculations are run first to determine the transient temperatures in the structure subjected to fire or data recorded during experiment can be used. Then, the mechanical analysis is performed in a step-by-step procedure consisting of subsequent static analyses or of a dynamic analysis, using the input temperature field. This procedure allows modeling of the mechanical behavior of a structure during the different stages of the fire (pre-flashover, post-flashover, and decay).

Civil engineering structures can usually be meshed using beams, trusses, and shells. A quadrilateral nonlinear thin shell element has been introduced in this software. Jetteur first developed this element in the room temperature program FINELG (originally developed by de Ville at the University of Liege and the Bureau d'Etudes Greisch). It has received the required modifications needed for high temperatures situation. This element, its capabilities and some validation examples are presented in this article.

FORMULATION OF THE SHELL ELEMENT

This element is based on the element developed by Jetteur [1-5] that has been implemented into the program FINELG.

Reference Configuration

For this non-planar quadrilateral element the z-axis is obtained as shown in Figure 1. a, b, c and d are the middle edge points (Figure 1), not necessarily coplanar. The z-axis is defined as:

$$\underline{z} = \frac{(\underline{db} \wedge \underline{ac})}{\|\underline{db} \wedge \underline{ac}\|} \tag{1}$$

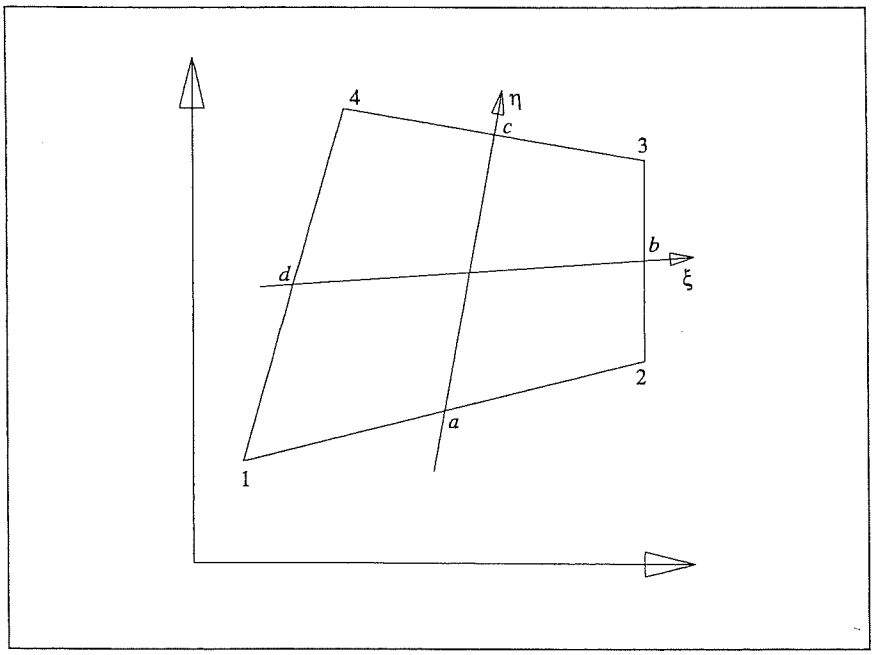

Figure 1. Reference configuration.

Another way to define the z-axis could be to find the best plane reference for the element:

$$w_0 = \alpha_1 + \alpha_2 x + \alpha_3 y \tag{2}$$

It can be shown that, if the coefficients α_2 and α_3 are chosen in such a way that the orientation of the reference plane minimizes the slopes between the element and the plane, then the z-axis defined by equation 1 is perpendicular to the plane. This proves that equation 1 minimizes also the slopes.

In equation 2, α_1 is still undetermined. It will be chosen in such a way that the plane of reference goes through the center of gravity of the quadrangle.

As it will be seen later, the membrane strains are not complete polynomials, so the results will be dependent on the choice of the x, y local axis. The angle between the x-axis and $\underline{bd}$ is imposed to be equal to the angle between $\underline{ac}$ and the y-axis (Figure 2). This determines the choice of the x, y-axis. For a rectangular element, this gives local axes parallel to the edges.

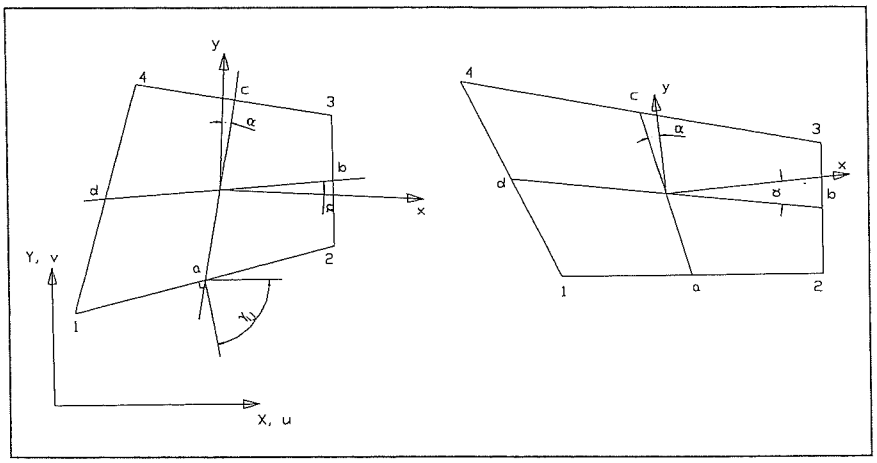

Figure 2. Local axes *x* and *y*.

The Membrane Behavior

The classical quadratic membrane displacement field is enlarged to cubic degree by means of cubic (along ξ and η) functions and constants A_{ij}. The development is similar to the one found in ALLMAN [6] for a triangle element.

$$u=\frac{1}{4}\left[\sum_{k=1}^{4}(1+\xi\xi_k)(1+\eta\eta_k)u_k+\sum_{sides}\phi_{ij}l_{ij}\cos\gamma_{ij}(\omega_j-\omega_i)+\sum_{sides}\psi_{ij}l_{ij}\cos\gamma_{ij}A_{ij}\right]$$

$$v=\frac{1}{4}\left[\sum_{k=1}^{4}(1+\xi\xi_k)(1+\eta\eta_k)v_k+\sum_{sides}\phi_{ij}l_{ij}\sin\gamma_{ij}(\omega_j-\omega_i)+\sum_{sides}\psi_{ij}l_{ij}\sin\gamma_{ij}A_{ij}\right] \quad (3)$$

$$\phi_{12}=\frac{1}{16}(1-\xi^2)(1-\eta) \qquad \psi_{12}=\frac{1}{8}(1-\xi^2)(1-\eta)\xi\eta^2$$

$$\phi_{23}=\frac{1}{16}(1+\xi)(1-\eta^2) \qquad \psi_{23}=\frac{1}{8}(1+\xi)(1-\eta^2)\xi^2\eta \quad (4)$$

$$\phi_{34}=\frac{1}{16}(1-\xi^2)(1+\eta) \qquad \psi_{34}=\frac{1}{8}(1-\xi^2)(1+\eta)\xi\eta^2$$

$$\phi_{41}=\frac{1}{16}(1-\xi)(1-\eta^2) \qquad \psi_{41}=\frac{1}{8}(1-\xi)(1-\eta^2)\xi^2\eta$$

$$l_{ij}=\sqrt{(x_j-x_i)^2+(y_j-y_i)^2} \quad (5)$$

$$A_{ij} = \frac{w_i + w_j}{2} + \frac{B_{ij} + B_{ji}}{2} \tag{6}$$

ω_i is the rotation at node i and ω_j is the rotation at node j. γ_{ij} is the direction of the outward normal along the edge ij. If $i = 1$ and $j = 2$ then B_{ij} and B_{ji} are equal to (for the complete definition, see Jaamei [7]):

$$B_{12} = \frac{1}{4J_1}(x_{41}u_1 + x_{14}u_2 + y_{41}v_1 + y_{14}v_2) \tag{7}$$

$$B_{21} = \frac{1}{4J_2}(x_{23}u_1 + x_{32}u_2 + y_{23}v_1 + y_{32}v_2) \tag{8}$$

$$J_1 = \frac{1}{4}(x_{21}y_{41} - x_{41}y_{21}) \tag{9}$$

$$J_2 = \frac{1}{4}(x_{21}y_{32} - x_{32}y_{21}) \tag{10}$$

The functions ψ_{ij} are chosen to be orthogonal to ϕ_{ij} with respect to integration over the quadrangle.

To improve the convergence, the shear strains are assumed to be constant over the element. After some calculation, the following equations are found:

$$\begin{aligned}
\varepsilon_x &= \frac{1}{8J}[(y_{42}u_{31} - y_{31}u_{42}) + \xi(y_{21}u_{43} - y_{43}u_{21}) + \eta(y_{41}u_{32} - y_{32}u_{41})] \\
\varepsilon_y &= \frac{1}{8J}[(v_{42}x_{31} - v_{31}x_{42}) + \xi(v_{21}x_{43} - v_{43}x_{21}) + \eta(v_{41}x_{32} - v_{32}x_{41})] \\
\bar{\gamma} &= \frac{1}{8J_0}[(u_{42}x_{31} - u_{31}x_{42}) + (y_{42}v_{31} - y_{31}v_{42})]
\end{aligned} \tag{11}$$

J is the determinant of the Jacobian matrix, J_0 is the value of J at $\xi = \eta = 0$ and x_{3l} is $x_3 - x_l$

Flexural Behavior

The formulation used is a Discrete Kirchhoff theory Quadrangular (DKQ). This element is fully described in [8-11]. The principle of this element will be briefly recalled here. The presentation is slightly different from the one given in [8-10].

The out-of-plane displacement and the rotations are parabolic over each side:

$$w = \sum_{i=1}^{8} N_i w_i \qquad \beta_x = \sum_{i=1}^{8} N_i \theta_{yi} \qquad \beta_y = \sum_{i=1}^{8} N_i \theta_{xi} \tag{12}$$

N_i are the shape functions and they depend on the parametric coordinates ξ and η. Along the side i, the out-of-plane displacement is given by:

$$w = -\xi\frac{(1-\xi)w_A}{2} + (1-\xi^2)w_C + \frac{\xi(1+\xi)w_B}{2} \tag{13}$$

w_A, w_B, and w_C are the normal displacements along z-axis normal to x-y plane (at the points A, B, and C). If we look at one edge of the element, for example, the edge from node 1 to node 2, node 1 is called A, node 2 is called B, and the middle point is called C (see Figure 3).

The contribution of the shear strain energy is neglected.

To reproduce thin plate theory, the Kirchhoff condition is imposed at selected points. In this element, the Kirchhoff constraints are imposed along the edges. The shear strain γ_{sz} at each of the two Gauss integration points along the sides is set to zero. Or, it is the same, as weighted averages of the shear strain are set to zero:

$$\int_l \gamma_{sz}\, ds = 0 \qquad \int_l \gamma_{sz}\, s\, ds = 0 \tag{14}$$

Moreover, the rotation around the side θ_s is imposed to vary linearly.

$$w_{,s} = \frac{-(1-2\xi)w_A + 4\xi w_C + (1+2\xi)w_B}{l} \tag{15}$$

In Plane Rotation

The in plane rotation or sixth degree of freedom of this element is described by Jetteur [12] and Jaamei [13]. A common method used to calculate the in-plane stiffness is to adjoin a small stiffness to this DOF (Degree Of Freedom). As it

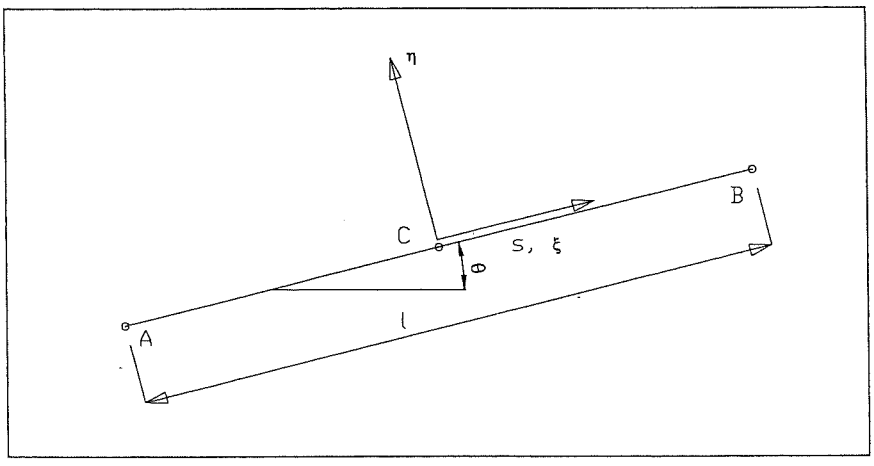

Figure 3. Local axis on one side.

can lead to wrong results, this method has been disregarded and it has been decided to include the in-plane rotation as an effective DOF [12, 13]. The approach followed for this element is very similar to the one used by Allman [6], Carpenter [14], and Taylor and Simo [15].

The interaction between the membrane stiffness (linked to the rotation ω) and the flexural coefficients generates an over-stiffness that slows down the convergence of the calculations and by the way increases the computational time. To reduce the stiffness of the element it is possible to introduce bubble modes but the simplicity of the element vanishes. A reduced integration scheme could have been used but it leads to a too soft element. The method selected for this element can be considered as a stabilization technique. The part field function of ω, in $\varepsilon_{ij}(\omega)$ (strains computed from the displacements), is amputated of its mean over the area A of the element, to overcome this excess of rigidity [12, 13]. In other words, the DOF ω has no longer any effect on constant strain modes.

General Features

The thickness is constant over the element. The integration on the surface is performed with a 2×2 points Gauss scheme. For the plain material that constitutes the element, the integration on the thickness is performed with a Gauss scheme using a user-defined number of points, from 2 if membrane behavior is dominant, up to 10 if bending is dominant.

Different layers of smeared re-bars with uniaxial behavior can be added to the plain material of the element. The contribution of these layers to the stiffness and internal forces is evaluated in the integration on the thickness, considering the exact position of each layer.

The usual situation encountered in reinforced concrete slabs is when the temperature varies through the thickness of the element. In that case, the temperature distribution comes from a SAFIR thermal analysis that has to be performed before the mechanical analysis. The temperature distribution on the thickness is the same at the four integration points. In steel structures, the thickness of the steel plates is such that the temperature distribution is nearly uniform on the thickness. On the other hand, a non-uniform distribution can appear in the planes of the plates. This is the case, for example, in an H section where the thickness of the web and of the flanges is different, which means different temperatures in the web and in the flanges because of different thermal massivity, and a transition zone in the region of the web to flanges connection. At the moment, it is possible to introduce in the structure a temperature field that depends on time and on the three global coordinates (plus, eventually the position in the thickness). This is done by a user-defined function that has to be programmed and compiled in a DLL file.

In the future, it is envisaged to develop the same numerical model in order to numerically determine the temperature distribution in the structure on the base of plate elements as the one used for the structural analysis.

MATERIAL PROPERTIES

The material properties of steel use the Von Mises criterion. The material properties of concrete use the Von Mises criterion in compression and a Rakine cut off in tension. The material properties decrease with temperature according to Eurocode 3 part 1.2 [16] for steel and Eurocode 2 part 1.2 [17] for concrete.

Steel

A temperature dependent plane stress associated plasticity model has been implemented to perform calculations on steel elements at elevated temperature. The limit surface is given by the Von Mises criterium.

The thermal strain is taken into account in SAFIR according to Eurocode 3 part 1.2 [16] and it is assumed to be hydrostatic (i.e., $\varepsilon_{thxx} = \varepsilon_{thyy} = \varepsilon_{th}$).

The elliptical law that is used for the isotropic hardening function is not exactly equal to the function defined as the stress-strain relationship at elevated temperature in the Eurocode 3 part 1.2 [16] (Figure 4-B.) Eurocode 3 defines the relationship in the σ-ε plane, whereas the present law is defined in the σ_{eq}-$\varepsilon_{pl,eq}$ plane (Figure 4-A.)

The hardening function is defined here as:

$$\sigma_{eq} = f_p \sqrt{b\left[1 - \frac{(\varepsilon_{pl,eq} - a)^2}{a^2}\right]} \tag{16}$$

$$a = 0.02 - f_y / E \qquad b = f_y - f_p$$

The following equations are used to calculate the yield strength, the Young's modulus and the proportional limit at elevated temperature:

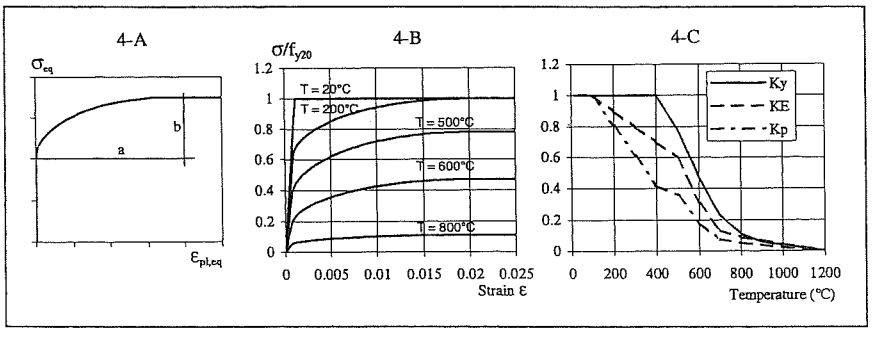

Figure 4. Elliptic hardening, σ-ε at elevated temperature and reduction coefficients for steel.

$$\sigma_{y,\theta} = k_{y,\theta}\sigma_{y,20} \qquad E_\theta = k_{E,\theta}E_{20} \qquad \sigma_{p,\theta} = k_{p,\theta}\sigma_{y,20}$$

The coefficients $k_{y,\theta}$, $k_{E,\theta}$, and $k_{p,\theta}$ are defined in Eurocode 3 part 1.2 (Figure 4-C).

Concrete

It is essential to define a concrete model that is appropriate for modeling the experimentally observed behavior of concrete slabs subjected to fire. The model must encompass every aspect that really influences the behavior of the structure, either one-way or two-way slabs, and be simple enough in order to allow simulations to be performed at a reasonable cost if the software is to be applied in civil engineering applications. The definition is based on the following considerations:

- Even if thermal gradients appear on the thickness, this does not generate any stress perpendicular to the plane of the shell and a plane stress model is still appropriate, as it was for the shell at room temperature or under elevated uniform temperature.
- Representation of the elasticity of the material is a minimum requirement in any element if a stiffness matrix has to be built.
- Concrete is known to have a poor behavior when submitted to tension and this must absolutely be represented. A simple Rankine tension cut off has been implemented here. Two points require further discussion.
  a) This criterion may be regarded as a crude representation of the real concrete behavior especially in the tension-compression regime. It is anyway considered to be acceptable for usual building reinforced concrete slabs in which the tension strength is not supposed to be provided by the concrete but, on the other hand, by steel re-bars. It has to be realized that this criteria should be refined if the element had to be used, for example, for the modeling of shear walls subjected to fire.
  b) It has been shown by comparison with experimental tests that laboratory results are better represented when a certain amount of tension strength is introduced in the model [18, 19]. For practical design applications yet, it is recommended to use zero as tension strength, and this is also a justification why the simple Rankine criteria may be acceptable. The reasons for designing with a zero tension strength are:
     » In a real building, the slab has encountered before the day of the fire a history of various thermal and loading cycles that have induced in the structure a significant amount of cracking, the level of which can hardly be estimated deterministically.
     » Shrinkage of concrete in the reinforced slab during the period that precedes the fire can also lead to tension stresses and hence cracking in the concrete.
     » If building structures were designed on the base of "a zero" tension strength at room temperature as a safe approximation, it would be even

unsafe to rely on tension strength of concrete at elevated temperature to ensure the stability of a building. This is because tension strength in concrete decreases faster with temperature increase than other material properties such as compressive strength of concrete or yield strength in steel bars [20].

- Because of the transient nature of thermal strains in a concrete slab during a fire, several integration points in the structure usually see their situation changing from tension to compression and vice versa. It is thus essential that the closing of cracks be treated appropriately. This is the case if tension is treated in the frame of plasticity; when the equilibrium point goes back to compression strains after cracking in tension, a new elastic loading in compression can be undertaken.
- Because of the poor behavior of concrete in tension, tension forces must be supported in the finite element by the steel bars. Smeared layers of steel bars have been embedded in the finite element. These bars develop stiffness and stress only in the direction of their axis. In other words, only an elongation in the direction of their axis will produce a stress while an elongation perpendicular to the axis or a shear strain in the element do not produce any stress in the bars.
- It has been shown in experimental tests that the behavior of two-way slabs under fire is predominantly influenced by the large deflection that arise [21, 22]; the transmission of the applied loads changes from a bending mode at room temperature to a tension membrane mode during the fire. This mode of load transmission can only be activated if the large displacements are represented, and these large displacements are mainly produced by the thermal strains. It is therefore essential, if two-way slabs are to be modeled, that the thermal strains be taken into account. A hydrostatic isotropic thermal strain has been embedded in the concrete model. The recommendation of Eurocode 2 [17] and Eurocode 3 [16] give the non-linear temperature dependency of the thermal strain for concrete and for steel. Of course, the thermal strain will also influence the displacements and the stress pattern in one-way slabs, but this is not so crucial as in two-way slabs.
- The amplitude of the displacements and the stress distribution will also be somewhat influenced by the stiffness of concrete in compression and this one decrease with a temperature increase. It is therefore worth incorporating this temperature dependency and, hence, have a thermo-elastic behavior in compression. This may have a significant effect, especially in continuous slabs, because the compression zone is the heated zone near the intermediate support and much less effect in simply supported slabs where the compression zone remains at rather low temperatures.
- For the same reason in continuous slabs, it may be worth limiting the amount of compression force that concrete is able to develop and, hence, to introduce a limit surface bounding the elastic domain. Because this is one of the most

widely used and tested surface, here concrete is supposed to be bounded by a Von Mises surface.

- Concrete in compression-compression is known to have a better behavior than what is predicted by the Von Mises surface. This is true at room temperature and this effect is even more pronounced at elevated temperature [23]. The Von Mises surface is anyway considered as a sufficiently good approximation because, in the fire situation, even the central zone of a two-way slab is not anymore submitted to a compression-compression situation; on the contrary, it is in a situation of tension-tension created by the membrane effect induced by large displacements. It also has to be considered that, among the various phenomena that have to be taken into account in the concrete model for the fire situation, crushing of concrete in compression is very low on the priority list. Anyway, it would not be a major difficulty to implement another failure surface, for example a Drücker-Prager surface, if the need arises in the future.

For reinforced concrete plates, to summarize, the contribution of the plain concrete is taken into account also by a temperature dependent Von Mises plane stress associated plasticity model on which a Rankine tension cut off has been added in tension; isotropic thermal strain is also taken into account.

The evolution of the Young's modulus and the curve for the isotropic hardenings are chosen in order to match as closely as possible the recommendations of Eurocode 2 for the uniaxial stress strain relationship of concrete.

Equation 17 gives the hardening function that has been chosen:

$$\left(\frac{3\varepsilon_{pl,eq} / \varepsilon_1 - 1)}{1.0004}\right)^2 + \left(\frac{\sigma_{eq}}{f_c}\right)^6 = 1 \tag{17}$$

This equation allows an elastic behavior up to $\sigma_{eq} = 0.305\, f_c$ and does not have an infinite slope at $\varepsilon_{pl,eq} = 0$.

ALGORITHMIC STRATEGY

The equilibrium of an integration point of the structure at the time 't' (step n) is represented by **A** on Figure 5. It is defined by:

If the initial strain $\{\varepsilon_i\}$ and the thermal strain $\{\varepsilon_{th,n}\}$ are subtracted from the total strain $\{\varepsilon_{tot,n}\}$, the mechanical strain $\{\varepsilon_{m,n}\}$ is obtained from:

$$\{\varepsilon_{m,n}\} = \{\varepsilon_{tot,n}\} - \{\varepsilon_i\} - \{\varepsilon_{th,n}\} \tag{18}$$

It is also possible to calculate the plastic strain, i.e., the mechanical strain that would exist in the structure if it was elastically unloaded. This is point **B** on Figure 5. Note that the unloaded structure is not equivalent to the initial structure (non-deformed). The equation is:

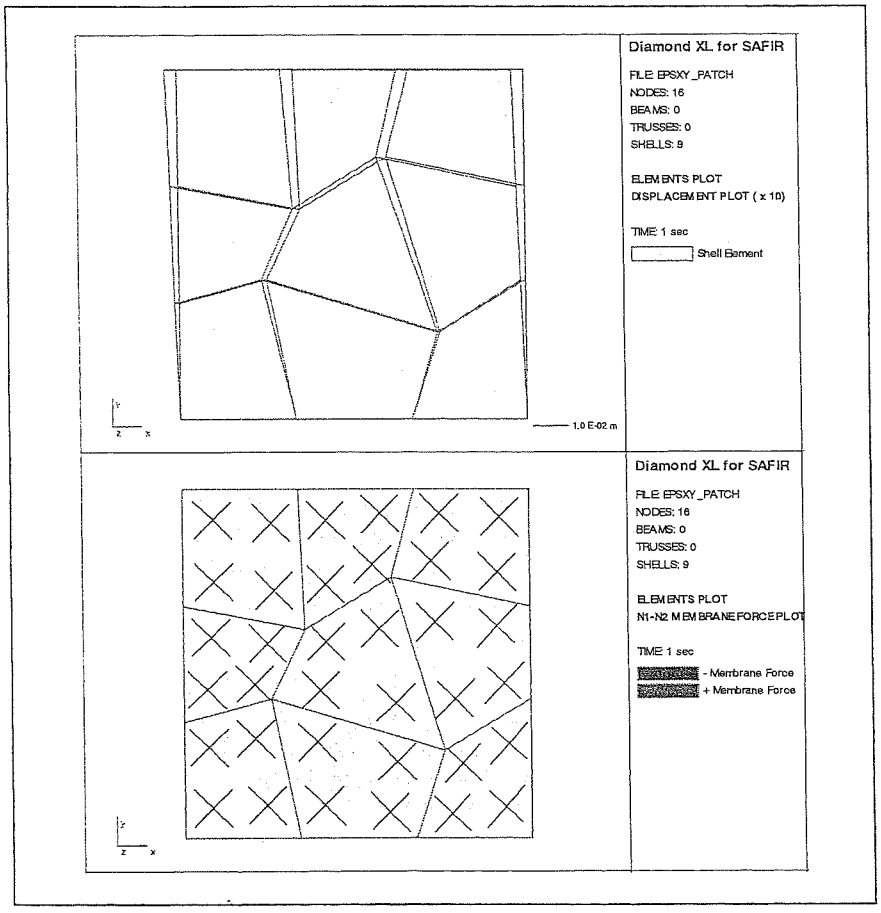

Figure 6. Cinematic patch test in shear.

given hereafter are consistent (i.e., they can be expressed in any system of units), provided that a single system is used. Whether the data are expressed in the international or in an Anglo-American system of units does not matter, the numbers that form results will be the same, expressed in the relevant system (except the temperature that should be expressed in degree Celsius.) The vertical and the horizontal members have a length of 120. Two meshes have been used to check the behavior in case of bending (shell elements in the x-y plane for the horizontal member and in the y-z plan for the vertical member) and in case of "membrane bending" (all the shell elements are in the x-z plane).

At the ends of the frame, the following displacements have been locked:

$$U_x = U_y = U_z = \theta_x = \theta_z = 0$$

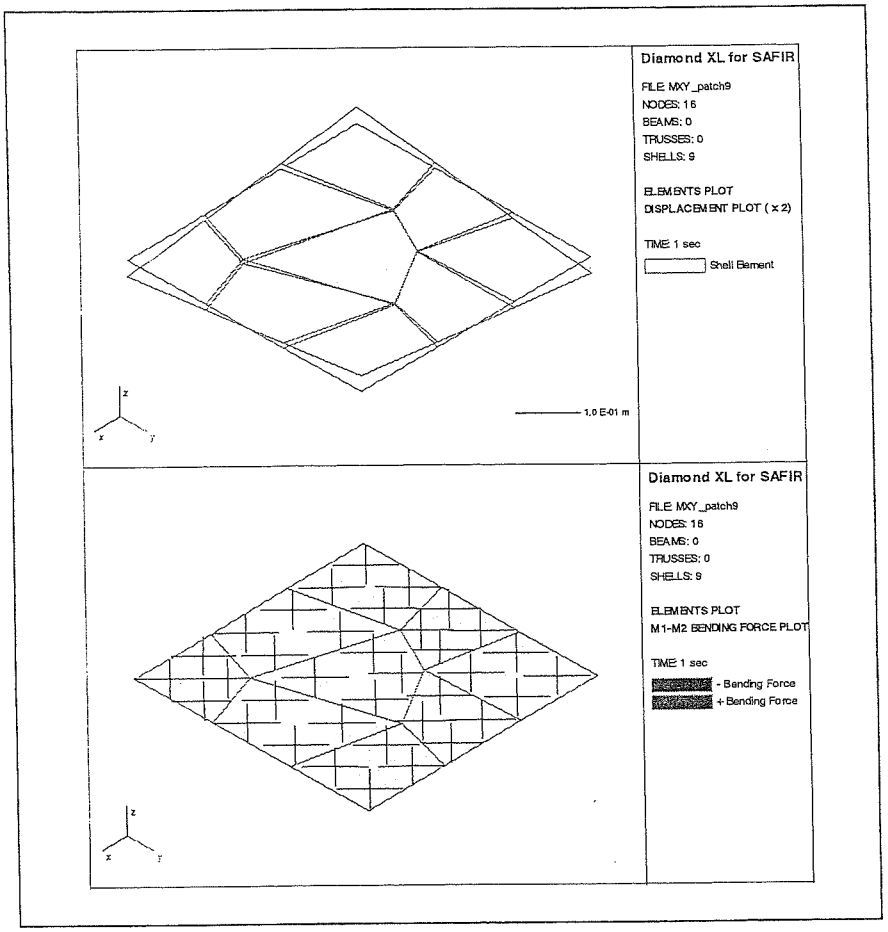

Figure 7. Cinematic patch test in torsion.

The cross-section of the beam is equal to 6 and the inertia is equal to 2. Eight-point Gauss integration points are used through the thickness of the elements. A vertical load of 0.2 is applied to the structure at a distance of 96 from the right top edge. The temperature is uniform in the structure and it is increased until collapse. At room temperature, the Young's modulus is equal to 720, the yield stress is equal to 3.0 and Poisson's ratio is equal to 0.3. The material properties decrease with temperature according to ENV 1993-1-2.

The results under fire condition have been compared with the same finite element programs as the ones used for the comparison at room temperature [24]. It can be seen (Figure 9) that in case of bending (SAFIR-Bending) the shell

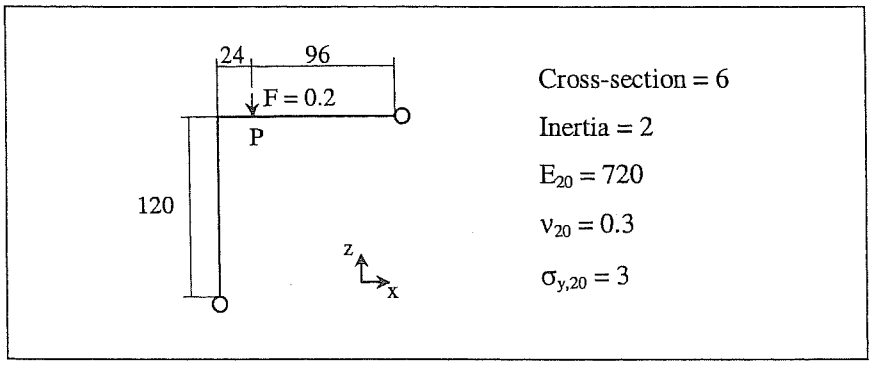

Figure 8. Lee's frame.

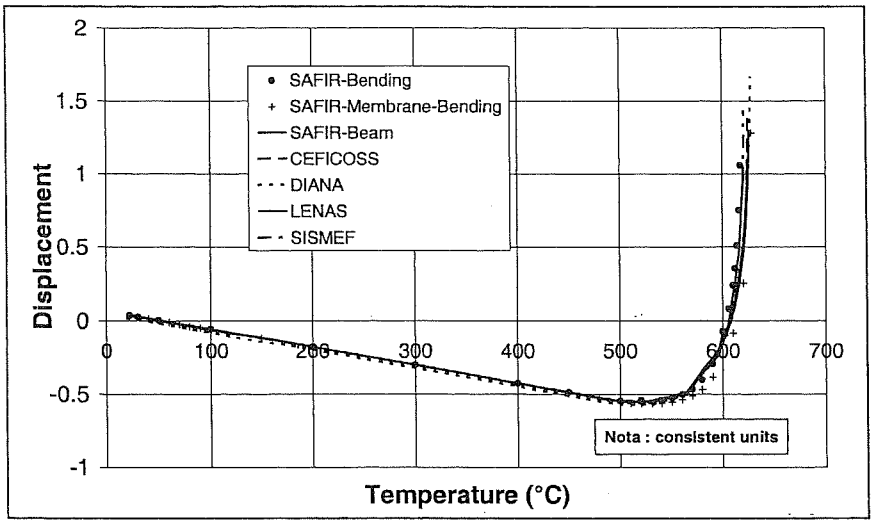

Figure 9. Horizontal displacement versus temperature.

element of SAFIR gives results close to the beam elements. In case of "membrane bending" (SAFIR-Membrane-Bending) the result is a little bit higher with the shell element than the results provided by the other elements. It has to be highlighted that the integration of plasticity on the depth of the beam is performed only at four integration points (two in each of the two elements used in the mesh).

This example shows that the new element takes correctly into account the thermal elongation and the stress-strain relationship according to Eurocode 3 part 1.2 [16].

CONCLUSION

The quadrilateral thin shell element introduced in SAFIR has been described and the material properties implemented in the program have been discussed. Some verification calculations have been performed and have shown that this element does not present any particular problem.

The element passes the cinematic patch tests at room temperature. Lee's frame at elevated temperature demonstrates that the material properties from Eurocode 3 part 1.2 [16] have accurately been introduced in SAFIR in case of plane stress relationship and that the thermal elongation is properly taken into account. It shows also that the shell element gives results that match the results obtained with beam elements (as this test was designed specifically for beam elements.)

To complete the verification and validation of the element, more calculations have to be done on benchmark tests at room and elevated temperature; comparisons with experimental tests have also to be performed.

The concrete model could be refined, especially for members where the behavior of concrete plays a crucial role, such as, for example, shear walls. An up-to-date model has been developed to investigate the behavior of concrete slabs (see companion article: Vol. 12, No. 1, "Nonlinear Thin Shell Finite Element for Steel and Concrete Structures Subjected to Fire: Verification and Validation") in bending as well as local instability in steel plates, as there was a specific demand for such analyses.

NOTATION

u, v : in plane node displacements
w : out of plane node displacement
ψ_{ij}, ϕ_{ij} : functions
J : determinant of the Jacobian matrix
A_{ij}, B_{ij} : matrix
ω_i : rotation of the node i
N_i : shape functions
ε, γ : strains
a, b : coefficients of the hardening function
f_y : ultimate strength
f_p : limit of proportionality
$\varepsilon_{pl,eq}$: equivalent plastic strain
$k_{y,\theta}$: reduction factor for ultimate strength at elevated temperature
$k_{E,\theta}$: reduction factor for Young's modulus at elevated temperature

$k_{p,\theta}$: reduction factor for proportional limit at elevated temperature
$f_{y,20}$: ultimate strength at room temperature
$f_{p,20}$: limit of proportionality at room temperature
E_{20} : Young's modulus at room temperature
E^*_{20} : tangent modulus at room temperature
$f_{y,\theta}$: ultimate strength at elevated temperature (θ)
$f_{p,\theta}$: limit of proportionality at elevated temperature (θ)
E_θ : Young's modulus at elevated temperature (θ)
E^*_θ : tangent modulus at elevated temperature (θ)
f_c : concrete compressive strength
t_n : time
T_n : temperature at the time t_n
$\varepsilon_{pl,eq,n}$: equivalent plastic strain
$\{\sigma_n\}$: stress vector
$\{\varepsilon_{tot,n}\}$: total strain vector
$\{\varepsilon_i\}$: initial strain vector
$\{\varepsilon_{th,n}\}$: thermal strain vector
$\{\varepsilon_{m,n}\}$: mechanical strain vector
$\{\varepsilon_{pl,n}\}$: plastic strain vector
$[D_n]$: elastic constitutive matrix
$\{\varepsilon^1_{tot,n+1}\}$: total strain vector of the first iteration of the time step $n+1$
$\{\varepsilon^1_{m,n+1}\}$: mechanical strain vector of the first iteration of the time step $n+1$
$\{\Delta\varepsilon^1\}$: first strain increment (first iteration)
$\{\Delta\varepsilon^2\}$: second strain increment (second iteration)
$\{\Delta\varepsilon^{1-2}\}$: strain increment between the first and second iteration

REFERENCES

1. FINELG, *Nonlinear Finite Element Analysis Program—User's Manual Version 6.2,* February 1984.
2. P. Jetteur, *Non-Linear Shell Elements Based on Marguerre Theory: IREM Internal Report 85/5,* Swiss Federal Institute of Technology, Lausanne, Switzerland, December 1985.
3. P. Jetteur, *A Shallow Shell Element with in-Plane Rotational Degrees of Freedom: IREM Internal Report 86/3,* Swiss Federal Institute of Technology, Lausanne, Switzerland, March 1986.
4. P. Jetteur, *Improvement of the Quadrangular "JET" Shell Element for a Particular Class of Shell Problems: IREM Internal Report 87/1,* Swiss Federal Institute of Technology, Lausanne, Switzerland, February 1987.
5. S. Jaamei, F. Frey, and P. Jetteur, *Elément Fini de Coque Mince Non-Linéaire à Six Degrés de Liberté par Noeud: IREM Internal Report 87/10,* Swiss Federal Institute of Technology, Lausanne, Switzerland, November 1987.
6. D. J. Allman, A Compatible Triangular Element Including Vertex Rotations for Plane Elastic Analysis, *Computer Structure, 19,* pp. 1-8, 1984.

7. S. Jaamei, *"JET" Thin Shell Finite Element with Drilling Rotations: IREM Internal Report 88/7,* Swiss Federal Institute of Technology, Lausanne, Switzerland, July 1988.
8. S. Idelsohn, *Analyses Statique et Dynamique des Coques par la Méthode des Eléments Finis,* Ph.D. thesis, Liege, 1974.
9. J. L. Batoz, K. J. Bathe, and L. W. Ho, A Study of Three Node Triangular Plate Bending Elements, *International Journal of Numeral Method Engingeering, 15,* pp. 1771-1812, 1980.
10. J. L. Batoz, An Explicit Formulation for an Efficient Triangular Plate Bending Element, *International Journal of Numeral Method Engineering, 18,* pp. 1077-1089, 1982.
11. J. L. Batoz and M. Ben Tahar, Evaluation of a New Quadrangular Thin Plate Bending Element, *International Journal of Numeral Method Engingeering, 18,* pp. 1655-1677, 1982.
12. P. Jetteur and F. Frey, A Four Node Marguerre Element for Non-Linear Shell Analysis, *Engineering Computations, 3*:4, pp. 276-282, 1986.
13. S. Jaamei, F. Frey, and P. Jetteur, Nonlinear Thin Shell Finite Element with Six Degrees of Freedom per Node, *Computer Methods in Applied Mechanics and Engineering, 75*:1-3, pp. 251-266, 1989.
14. N. Carpenter, H. Stolarsky, and T. Belytschko, Flat Triangular Shell Element with Improved Membrane Interpolation, *Communications in Applied Numerical Methods, 1*:4, pp. 161-168, 1985.
15. R. Taylor and J. C. Simo, Bending and Membrane Elements for Analysis of Thick and Thin Shell, *Proceedings NUMETA 1985 Conference,* Swansea, pp. 587-591, 1985.
16. CEN ENV 1993-1-2, *Eurocode 3, Design of Steel Structures, Part 1.2, General Rules, Structural Fire Design,* European Committee for Standardization, Belgium, 1995.
17. CEN ENV 1992-1-2, *Eurocode 2, Design of Concrete Structures, Part 1.2, General Rules, Structural Fire Design,* European Committee for Standardization, Belgium, 1994.
18. L. Lim, *Membrane Action in Fire Exposed Concrete Floor Systems,* Ph.D. thesis, Department of Civil Engineering, University of Canterbury, New Zealand, 2003.
19. L. Lim, A. Buchanan, and P. Moss, Behaviour of Simply-Supported Two-Way Reinforced Concrete Slabs in Fire, *Proceedings of "Designing Structure for Fire,"* SFPE, pp. 227-236, 2003.
20. U. Schneider, *Properties of Materials at High Temperatures: Concrete,* Department of Civil Engineering, Gesamthochschule Kassel, 1985.
21. M. Gillie, A. S. Usmani, and J. M. Rotter, A Structural Analysis of the Cardington British Steel Corner Test, *Journal of Construction Steel Research, 58,* pp. 427-442, 2002.
22. A. Usmani, Understanding the Response of Composite Structures to Fire, *Proceedings of NASCC,* Section D5, A.I.S.C. Inc., 2003
23. C. Ehm, *Versuche zür Festichkeit und Verformung von Beton unter Zweiaxialer Beanspruchung und höhen Temperaturen,* Ph.D. thesis, Inst. Fr Baustoffe, Massivbau and Brandschutz, Technischen Universität Braunschweig, 1986.

24. J. M. Franssen et al., A Comparison between Five Structural Fire Codes Applied to Steel Elements, *Proceedings of the Fourth International Symposium, IAFSS, Fire Safety Science,* 1984.

Direct reprint requests to:

Didier Talamona
University of Ulster, Jordanstown
Newtownabbey, Country Antrim, BT370QB
Northern Ireland
e-mail: d.talamona@ulster.ac.uk